

# Analysis of Resonance Multipoles from Polarization Observables in Eta Photoproduction

L. Tiator, D. Drechsel and G. Knöchlein

*Institut für Kernphysik, Johannes Gutenberg-Universität, D-55099 Mainz, Germany*

C. Bennhold

*Center for Nuclear Studies, Department of Physics, The George Washington University, Washington, D.C., 20052*

(February 9, 2008)

A combined analysis of new eta photoproduction data for total and differential cross sections, target asymmetry and photon asymmetry is presented. Using a few reasonable assumptions we perform the first model-independent analysis of the  $E_{0+}$ ,  $E_{2-}$  and  $M_{2-}$  eta photoproduction multipoles. Making use of the well-known  $A_{3/2}$  helicity amplitude of the  $D_{13}(1520)$  state we extract its branching ratio to the  $\eta N$  channel,  $\Gamma_{\eta N}/\Gamma = (0.08 \pm 0.01)\%$ . At higher energies, we show that the photon asymmetry is extremely sensitive to small multipoles that are excited by photons in the helicity  $3/2$  state. The new GRAAL photon asymmetry data at higher energy show a clear signal of the  $F_{15}(1680)$  excitation which permits extracting an  $F_{15}(1680) \rightarrow \eta N$  branching ratio of  $(0.15^{+0.35}_{-0.10})\%$ .

PACS numbers: 13.60.Le, 14.20.Gk, 13.75.Gx

*Keywords:* eta production,  $S_{11}(1535)$ ,  $D_{13}(1520)$ ,  $F_{15}(1680)$

## I. INTRODUCTION

Over the past years, eta photoproduction has demonstrated its potential as a new, powerful tool to selectively probe certain resonances that are difficult to explore with pions. It is well known that the low energy behavior of the eta production process is governed by the  $S_{11}(1535)$  resonance [1–3]. The recent, precise measurements of total and differential cross sections for eta photoproduction at low energies [4,6] have made it possible to determine the  $S_{11}(1535)$  resonance parameters with unprecedented precision. A well-known example of the power of the  $(\gamma, \eta)$  reaction is the extraction of the  $A_{1/2}^p$  helicity amplitude of the  $S_{11}(1535)$  state. Due to the combined cusp-resonance nature of this resonance, analyses based solely on pion photoproduction consistently underestimate this quantity with values of about  $60 \cdot 10^{-3} GeV^{-1/2}$  [7], while extractions from eta photoproduction result in numbers nearly twice as high [4]. Recent coupled-channels analyses [8,9] that properly include cusp as well as resonance phenomena have confirmed a range of values consistent with eta photoproduction.

However, because of the overwhelming dominance of the  $S_{11}$  the influence of other resonances in the same energy regime, such as the  $D_{13}(1520)$ , is difficult to discern. It has been pointed out [2] that polarization observables provide a new doorway to access these non-dominant resonances by use of interference of the dominant  $E_{0+}$  multipole with the smaller multipoles. In particular, the polarized photon asymmetry was shown to be sensitive to the  $D_{13}(1520)$ . It is well-known that, in principle, for a completely model-independent multipole analysis seven single and double polarization observables have to be measured along with the differential cross section for all isospin channels. However, in practice, the recent extraction of the small  $E_{1+}^{3/2}$  multipole at the  $\Delta(1232)$  energy [11] demonstrates that the use of a few reasonable assumptions permits an almost model-independent analysis with a restricted set of observables for a limited energy range.

Recently, polarization data for the target and photon asymmetries in eta photoproduction were measured at ELSA [10] and GRAAL [12], respectively, for the first time. Combining these data with the unpolarized cross sections from MAMI, we have performed an almost model-independent multipole analysis of the  $l = 0$  and 2 eta photoproduction multipoles at threshold. This permits a precise determination of the  $D_{13}(1520)$  contribution and an extraction of new  $D_{13}(1520)$  resonance parameters.

## II. MULTIPOLE ANALYSIS

The three measured observables are represented by the response functions of [13] as follows:

$$\frac{d\sigma}{d\Omega} = \frac{q_\eta}{k} R_T^{00}, \quad (1)$$

$$T = \frac{R_T^{0y}}{R_T^{00}}, \quad (2)$$

$$\Sigma = -\frac{{}^c R_{TT}^{00}}{R_T^{00}}, \quad (3)$$

where  $q_\eta$  and  $k$  are the absolute values of the eta and photon momenta, respectively, and here and in the following all variables are expressed in the *cm* frame.

Because of the overwhelming dominance of the  $S_{11}$  channel in eta photoproduction, these observables can be expressed in terms of *s*-wave multipoles and interferences of the *s* wave with other multipoles. In the CGLN basis this leads to an  $F_1$  dominance and the observables can simply be expressed as

$$R_T^{00} = |F_1|^2 - \text{Re} \{ 2 \cos \theta F_1^* F_2 - \sin^2 \theta F_1^* F_4 \}, \quad (4)$$

$$R_T^{0y} = 3 \sin \theta \text{Im} \{ F_1^* F_3 + \cos \theta F_1^* F_4 \}, \quad (5)$$

$${}^c R_{TT}^{00} = \text{Re} \{ F_1^* F_4 \}, \quad (6)$$

where  $\theta$  is the scattering angle. If we retain only interferences with *p* and *d* waves (an approximation valid at least up to 1 GeV photon *lab* energy) we obtain

$$\begin{aligned} R_T^{00} &= |E_{0+}|^2 - \text{Re} [E_{0+}^* (E_{2-} - 3M_{2-})] \\ &\quad + 2 \cos \theta \text{Re} [E_{0+}^* (3E_{1+} + M_{1+} - M_{1-})] \\ &\quad + 3 \cos^2 \theta \text{Re} [E_{0+}^* (E_{2-} - 3M_{2-})], \end{aligned} \quad (7)$$

$$\begin{aligned} R_T^{0y} &= 3 \sin \theta \text{Im} [E_{0+}^* (E_{1+} - M_{1+})] \\ &\quad - 3 \sin \theta \cos \theta \text{Im} [E_{0+}^* (E_{2-} + M_{2-})], \end{aligned} \quad (8)$$

$${}^c R_{TT}^{00} = -3 \sin^2 \theta \text{Re} [E_{0+}^* (E_{2-} + M_{2-})]. \quad (9)$$

Using the angle-independent quantities

$$a = |E_{0+}|^2 - \text{Re} [E_{0+}^* (E_{2-} - 3M_{2-})], \quad (10)$$

$$b = 2 \text{Re} [E_{0+}^* (3E_{1+} + M_{1+} - M_{1-})], \quad (11)$$

$$c = 3 \text{Re} [E_{0+}^* (E_{2-} - 3M_{2-})], \quad (12)$$

$$d = \frac{3}{a + c/3} \text{Im} [E_{0+}^* (E_{1+} - M_{1+})], \quad (13)$$

$$e = -\frac{3}{a + c/3} \text{Im} [E_{0+}^* (E_{2-} + M_{2-})], \quad (14)$$

$$f = \frac{3}{a + c/3} \text{Re} [E_{0+}^* (E_{2-} + M_{2-})], \quad (15)$$

we can express the observables by a power series in  $\cos \theta$  that can be fitted to the experimental data at various energies

$$\frac{d\sigma}{d\Omega} = \frac{q_\eta}{k} (a + b \cos \theta + c \cos^2 \theta), \quad (16)$$

$$T = \sin \theta (d + e \cos \theta), \quad (17)$$

$$\Sigma = f \sin^2 \theta. \quad (18)$$

Quite remarkable, a combined analysis of these three observables allows a determination of the *d*-wave contributions to eta photoproduction once the quantities *a*, *c*, *e* and *f* have been determined from experiment. As was already pointed out in Ref. [4], the differential cross section alone determines the magnitude of the *s*-wave multipole

$$|E_{0+}| = \sqrt{a + \frac{c}{3}} = \sqrt{\frac{1}{4\pi} \frac{k}{q_\eta} \sigma_{total}}. \quad (19)$$

With the knowledge of *e* and *f* the helicity 3/2 multipole  $B_{2-}$ , defined below, and the phase relative to the  $S_{11}$  channel can be determined:

$$|B_{2-}| \equiv |E_{2-} + M_{2-}| = \frac{1}{3} \sqrt{(e^2 + f^2)(a + c/3)}, \quad (20)$$

$$\tan(\phi_{E_{0+}} - \phi_{B_{2-}}) = \frac{e}{f}. \quad (21)$$

As is well known the pion photoproduction  $E_{1+}$  and  $M_{1+}$  multipoles in the  $\Delta(1232)$  region must have the same phase due to the Watson theorem. For resonances at higher energies this relation does not hold anymore since other channels are open and background rescattering can affect the phases of the electric and magnetic multipoles in a different way. Neglecting such effects for now,  $\phi_{E_{\ell\pm}} = \phi_{M_{\ell\pm}} = \phi_{\ell\pm}$ , we arrive at

$$E_{\ell\pm} = |E_{\ell\pm}| e^{i\phi_{\ell\pm}}, \quad (22)$$

$$M_{\ell\pm} = |M_{\ell\pm}| e^{i\phi_{\ell\pm}}, \quad (23)$$

with the following expressions for the magnitudes of the  $l = 2$  multipoles:

$$|A_{2-}| = \frac{1}{2} |3M_{2-} - E_{2-}| = -\frac{c}{6f} \sqrt{\frac{e^2 + f^2}{a + c/3}}, \quad (24)$$

$$|E_{2-}| = \frac{1}{4} \sqrt{\left(a + \frac{c}{3}\right) (e^2 + f^2)} \left|1 + \frac{c}{3f(a + c/3)}\right|, \quad (25)$$

$$|M_{2-}| = \frac{1}{12} \sqrt{\left(a + \frac{c}{3}\right) (e^2 + f^2)} \left|1 - \frac{c}{f(a + c/3)}\right|. \quad (26)$$

$$(27)$$

It is obvious from the data [4] that the total cross section can be perfectly fitted to a Breit-Wigner form in the region of the  $S_{11}(1535)$  resonance, which results in an  $s$ -wave dominated differential cross section. An investigation of the background due to the Born terms [2] yielded a very small eta-nucleon coupling constant, and this result was confirmed by more recent coupled-channels analyses [9]. As a consequence, the  $E_{0+}$  multipole can, to a high degree of accuracy, be solely described by the  $S_{11}(1535)$  contribution parameterized through a Breit-Wigner form [4]. The additional arbitrary phase of the complex  $E_{0+}$  multipole is usually set equal to zero by convention. If one uses a Breit-Wigner parameterization of the complex  $E_{0+}$  multipole, the phase  $\phi_{0+}$  is given by

$$\tan \phi_{0+}(W) = \frac{\Gamma(W)M_R}{M_R^2 - W^2}, \quad (28)$$

where  $W$  is the  $cm$  energy and  $M_R$  the mass of the resonance (conventional resonance position). The energy dependent width of the resonance is given by

$$\Gamma(W) = \Gamma_R \left( b_\eta \frac{q_\eta}{q_{\eta,R}} + b_\pi \frac{q_\pi}{q_{\pi,R}} + b_{\pi\pi} \right), \quad (29)$$

where  $b_\eta, b_\pi$  and  $b_{\pi\pi}$  denote the branching ratios into the  $\eta N$ ,  $\pi N$  and  $\pi\pi N$  channels, respectively.

The analysis of the interference between the  $E_{0+}$  and the  $E_{2-}$  and  $M_{2-}$  multipoles determines the  $d$ -wave multipoles and therefore the difference  $\phi_{2-} - \phi_{0+}$ . It does not yield direct information on  $\phi_{2-}$ . However, using the above assumptions for the  $E_{0+}$  multipole we can then obtain the phase  $\phi_{2-}$ . Alternatively, if we assume a Breit-Wigner shape for the  $D_{13}$  resonance multipoles, we can obtain the phase  $\phi_{0+}$ .

To perform a similar analysis of the  $p$ -wave multipoles requires more information from additional polarization observables; in particular, a measurement of the recoil polarization would be useful. As before, we obtain

$$P = \frac{R_T^{y0}}{R_T^{00}} = \sin \theta (h + k \cos \theta) \quad (30)$$

with

$$h = -\frac{1}{a + c/3} \text{Im} [E_{0+}^* (2M_{1-} + 3E_{1+} + M_{1+})], \quad (31)$$

$$k = 3 \frac{1}{a + c/3} \text{Im} [E_{0+}^* (E_{2-} - 3M_{2-})]. \quad (32)$$

In analogy to Eqs. (19, 20) we can determine the helicity 1/2 multipole  $A_{2-}$  of the  $D_{13}$  channel in a model-independent way,

$$|A_{2-}| \equiv \frac{1}{2}|3M_{2-} - E_{2-}| = \sqrt{\frac{c^2 + (a + c/3)^2 k^2}{a + c/3}}, \quad (33)$$

$$\tan(\phi_{A_{2-}} - \phi_{E_{0+}}) = \frac{(a + c/3)k}{c}. \quad (34)$$

Furthermore, together with Eqs. (11 and 13), the quantity  $h$  allows one to determine the resonance structure of the  $p$ -wave multipoles.

### III. RESULTS

#### A. Extraction of the multipoles

Fig. 1 shows 4 out of 10 angular distributions measured by the TAPS collaboration at Mainz [4] in the energy range between 716 and 790 MeV. While the isobar model of Ref. [13] falls somewhat low near threshold, a perfect fit is possible using the ansatz of Eq. (16). The coefficient  $a$  can be fitted to a Breit-Wigner form with an energy-dependent width leading, e.g., to  $M_R = (1549 \pm 8) \text{ MeV}$ ,  $\Gamma_R = (202 \pm 35) \text{ MeV}$  and an absolute value of the  $s$ -wave multipole at threshold,  $|E_{0+}| = 16 \cdot 10^{-3}/m_\pi^+$  (Fit 1, Ref. [4]). For our present purpose, however, it is more convenient to use a general polynomial expansion for the coefficients as described in Section III.C.

Fig. 2 shows our fit to the target polarization data from Bonn [10]. In this case the isobar model of Ref. [13] fails to reproduce the angular shape of the data. In particular, the model does not reproduce the node found experimentally at low energy. Furthermore, the model ingredients are quite insensitive to the  $D_{13}$  resonance. In previous coupled-channels analyses [1,2] the  $D_{13}$  resonance came out much stronger and a node developed. However, the node resulted in a negative asymmetry at forward and a positive asymmetry at backward angles, clearly opposite to the experimental observation and, as we shall see below, leading to a drastically different relative phase between  $s$  and  $d$  waves. Quite to the contrary, the ansatz of Eq. (17) does describe the data and leads to a node at energies below 800 MeV.

Fig. 3 compares our fit and the isobar model of Ref. [13] for the photon asymmetry. This observable has recently been measured at GRAAL [12] from threshold up to 1050 MeV. At the lower energies, the good agreement between the data and the isobar model illustrates the importance of the  $D_{13}(1520)$  resonance. Without the  $D_{13}$  the polarized photon asymmetry is almost zero for energies below 900 MeV and turns negative for the higher energies. With regard to our multipole analysis, Fig. 3 clearly demonstrates that we can achieve an excellent fit with the ansatz of Eq. (18). Up to 900 MeV the asymmetry has a clean  $\sin^2 \theta$  dependence and can be parameterized by a single energy-dependent parameter  $f$ . However, above 900 MeV the data show the evolution of a forward-backward asymmetry that becomes most pronounced at 1050 MeV. This behavior cannot be fitted any longer with the form of Eq. (18) but requires an additional coefficient,

$$\Sigma = \sin^2 \theta (f + g \cos \theta), \quad (35)$$

where  $g$  is determined solely by multipoles of order 3 and higher,

$$g = \frac{15}{a + c/3} \text{Re} [E_{0+}^* (E_{3-} + M_{3-} + E_{3+} - M_{3+})]. \quad (36)$$

The obvious need for the coefficient  $g$  at higher energies therefore represents a clear signal that partial waves beyond  $d$  waves are required by the photon asymmetry data.

#### B. The photon asymmetry at higher energies

As has been discussed above, eta photoproduction at low energies is dominated by  $s$  waves giving rise to essentially flat angular distributions with only small modulations as found by the Mainz precision experiment [4]. But also the angular distributions measured at Bonn up to 1.15 GeV [16] have given no evidence for a break-down of this  $s$ -wave dominance. This gives us the possibility to extract the small contributions of the higher resonances in exactly the same way as shown above for the  $D_{13}$  resonance, i.e. by analyzing the interference with the leading  $s$ -wave multipole.

In the following we shall demonstrate this method for the nucleon resonances with strong helicity 3/2 couplings  $A_{3/2}$ .

Assuming  $s$ -wave dominance, and therefore,  $F_1$ -dominance in the CGLN basis, we can derive a general expression for the photon asymmetry by using Eq. (6),

$$\begin{aligned}\Sigma(\theta) &= -\sin^2 \theta \operatorname{Re}[F_1^* F_4]/R_T^{00} \\ &= \sin^2 \theta \operatorname{Re}\left[E_{0+}^* \sum_{\ell \geq 2} (B_{\ell-} + B_{\ell+}) P_\ell''(\cos \theta)\right]/R_T^{00}\end{aligned}\quad (37)$$

with  $B_{\ell-} = E_{\ell-} + M_{\ell-}$  and  $B_{\ell+} = E_{\ell+} - M_{\ell+}$ .

Both multipole combinations have helicity 3/2 and, for resonance excitation, are proportional to the photon couplings  $A_{3/2}$ . The helicity 1/2 couplings  $A_{1/2}$  do not enter in Eq. (37) but only appear in the differential cross section and in the recoil polarization, e.g., as  $A_{2-} = (3M_{2-} - E_{2-})/2$ . Expanding to  $\ell_{max} = 4$ , we then obtain

$$\begin{aligned}\Sigma(\theta) &= \frac{\sin^2 \theta}{|E_{0+}|^2} \operatorname{Re}\left\{E_{0+}^* \left[3(B_{2-} + B_{2+}) - \frac{15}{2}(B_{4-} + B_{4+})\right.\right. \\ &\quad \left.\left.+ 15(B_{3-} + B_{3+}) \cos \theta + \frac{105}{2}(B_{4-} + B_{4+}) \cos^2 \theta\right]\right\}.\end{aligned}\quad (38)$$

This result demonstrates that any deviation from the  $\sin^2 \theta$  dependence in the photon asymmetry is due to  $f$  waves or higher partial waves. These could originate from either strong background contributions or resonances with spin 5/2 or higher. We point out that such contributions would appear in the differential cross section as  $\cos^3 \theta$  terms, which would be difficult to extract. Since the background contributions in eta photoproduction are known to be small, the only remaining option for these partial waves is a resonance with  $J \geq 5/2$ .

In Table I we list all entries for  $N^*$  resonances with isospin 1/2. From this table one finds the  $D_{13}$  as the strongest candidate that contributes significantly to the photon asymmetry. The next higher-lying resonance with a strong helicity 3/2 coupling is the  $F_{15}(1680)$ , which is known to play an important role in pion photoproduction. Since its mass matches the energy region of the forward-backward asymmetry in the photon polarization, we conclude that the GRAAL data reveal the presence of the  $F_{15}(1680)$  resonance in eta photoproduction. In section III.D we shall extract the  $\eta N$  branching ratio from this signal.

At even higher energies and beyond our present scope of interest, there are the less-established  $F_{17}(1990)$  and  $G_{17}(2190)$  whose properties could be extracted by measuring the photon asymmetry at the corresponding energies. We have verified that even if two small resonances of different multipolarity would be excited in the same energy region they will produce a clear signal allowing us to determine the  $\eta$  branching ratios down to values well below 0.1%. In Fig. 4 we demonstrate how such interferences of higher resonances with the  $S_{11}$ -channel would show up in the photon asymmetry.

### C. Parameterization of the multipoles

Fig. 5 compares the results of our multipole analysis with the isobar model calculation of Ref. [13]. The most dramatic difference occurs for the relative phase between the  $s$  and  $d$  waves. As shown in Eq. (21), this phase difference is model independent. If both the  $S_{11}(1535)$  and the  $D_{13}(1520)$  are parameterized by Breit-Wigner functions (as in the case of the isobar model [13]), this phase difference would be rather constant, because both resonances are very close in energy and, furthermore, have similar resonance widths. Since the  $S_{11}$  is a little bit higher in energy, the phase difference  $\phi_0 - \phi_2$  should be small and negative as shown by the dotted line in Fig. 5.

From the above analysis we conclude that this unexpected discrepancy is directly connected to the node structure in the target asymmetry. Without a node or with a node but an  $e$  coefficient of opposite sign, the phase difference would be much smaller and closer to our model calculations. Other models based on either a coupled-channels approach [9] or on a tree-level effective Lagrangian analysis [19], have similar problems to reproduce the target asymmetry. It is therefore imperative that this measurement be verified as soon as possible.

After performing single-energy fits we used a polynomial form for the energy dependence of the coefficients  $a$ ,  $b$ ,  $c$ ,  $d$ ,  $e$  and  $f$  of Eqs. (10)-(15) in order to arrive at a global (energy-dependent) solution for the multipoles. This has several advantages: First, the experimental data were obtained in different set-ups at different labs, thus their energy bins do not match. Second, except for the quantity  $a$  that can be determined already from the total cross section, all other quantities contain considerable error bars. Therefore, a combined fit can reduce the uncertainty of individual measurements considerably. In a simple Taylor expansion in terms of the eta momentum with only 1 to

3 parameters in each coefficient, we obtain good results for the energy region from threshold up to about 900 MeV. Using polynomials as a function of  $q_\eta/m_\eta$  as shown in Table II, we obtain very good fits in the complete energy range of the present experiments. In Table II we made use of the constraints for the threshold behavior of the multipoles, in particular the vanishing of the  $p$ -,  $d$ - and  $f$ -wave multipoles at threshold. In Figs. 6 and 7 we show our energy dependent fits to the coefficients  $a$  to  $g$  obtained at single energies. The coefficients of the differential cross section in Fig. 6 reproduce the findings of Krusche et al. [4], the dominance of the  $s$ -wave amplitude in the coefficient  $a$ , an  $s$ - $p$  interference compatible with zero in the coefficient  $b$ , and a small  $s$ - $d$  interference in the coefficient  $c$ . Fig. 7 shows the coefficients  $d$  to  $g$  obtained from fits to the target and photon asymmetries. In this case the coefficient  $e$  is not very well defined by the target asymmetry and our energy dependent fit gives just the most likely polynomial description. Finally, the strong rise in the coefficient  $g$  around 1 GeV shows the excitation of the  $F_{15}(1680)$  resonance, which was measured just up to the resonance peak expected at  $E_\gamma^{lab} = 1035$  MeV. An experiment at even higher energies is now in progress at GRAAL with the aim to confirm the resonance behavior.

#### D. Helicity amplitudes and branching ratios

With the definitions given in Appendix A we are now in a position to determine the helicity amplitudes and/or branching ratios. We present two separate analyses of resonance parameters based on two different assumptions: First, we perform a model-independent analysis that uses both the target asymmetry with coefficient  $e \cos \theta \sin \theta$  and the beam asymmetry with  $f \sin^2 \theta$ . Second, because of the fact that the phase difference  $\Delta\phi = \phi_0 - \phi_2$  is mainly due to the target asymmetry, we also perform an analysis ignoring the measurement of  $T$  and assuming a normal resonance behavior for the  $S_{11}(1535)$ , with a phase given by the Breit-Wigner form, Eq. (28).

According to appendix A the branching ratio is related to the photoproduction amplitude  $B_{2-}$  by

$$\sqrt{b_\eta} = \left( \frac{3\pi q_{\eta,R} M_R \Gamma_R}{k_R m_N} \right)^{1/2} \frac{\tilde{B}_{2-}}{A_{3/2}}, \quad (39)$$

where we have introduced  $b_\eta = \Gamma_\eta/\Gamma_R$ . In case 1 the amplitude  $\tilde{B}_{2-}$  is evaluated with Eq. (20), in case 2 we use

$$\tilde{B}_{2-} = \frac{\sqrt{a+c/3}}{\sin \delta_0} \frac{f}{3} \Big|_{W=1520 \text{ MeV}} \quad (40)$$

with  $\delta_0 = 72^\circ$  in contrast to  $136^\circ$  from our model-independent analysis (Fig. 4). Using Eq. (24) to evaluate the helicity 1/2 amplitude  $\tilde{A}_{2-}$  we can now determine the helicity ratio

$$\frac{A_{3/2}}{A_{1/2}} = -\frac{\sqrt{3}}{2} \frac{\tilde{B}_{2-}}{\tilde{A}_{2-}} = \sqrt{3} \frac{f}{c} \left( a + \frac{c}{3} \right), \quad (41)$$

independent of the target asymmetry measurement. Furthermore, the reduced photoproduction resonance parameters  $\xi_i$ , Eq. (A4), are simply related to the amplitudes  $A_{2-}, B_{2-}$  by

$$\xi_{1/2} = -\sqrt{4\pi} \tilde{A}_{2-} \quad \text{and} \quad \xi_{3/2} = -\sqrt{3\pi} \tilde{B}_{2-}. \quad (42)$$

For our analysis of the  $F_{15}(1680)$  resonance, there exists experimental information only on the photon asymmetry and the total cross section at 1 GeV. Therefore, only case 2 is applicable and we obtain

$$\sqrt{b_\eta} = \left( \frac{12\pi q_{\eta,R} M_R \Gamma_R}{k_R m_N} \right)^{1/2} \frac{\tilde{B}_{3-}}{A_{3/2}}, \quad (43)$$

$$\tilde{B}_{3-} = \sqrt{\frac{k_R \sigma_{total}}{4\pi q_{\eta,R}}} \frac{g}{15 \sin \delta_0} \Big|_{W=1680 \text{ MeV}}, \quad (44)$$

with  $\delta_0 = 137^\circ$  from Eq. (28). In the case of the  $F_{15}$  resonance we have no information on the helicity 1/2 amplitude  $A_{3-}$  and therefore  $A_{1/2}$  is not determined. This helicity amplitude is only crudely known from pion photoproduction. The value for  $\xi_{3/2}$  is obtained from

$$\xi_{3/2} = \sqrt{12\pi} \tilde{B}_{3-}. \quad (45)$$

In Table III we show our numerical results for the resonance parameters together with the values given by the Particle Data Tables [17] and a recent analysis of Mukhopadhyay and Mathur [19]. It is very interesting to note that though the  $D_{13}$  has a branching ratio of only 0.08% according to our analysis it nevertheless totally dominates the photon asymmetry as shown in Fig. 3. The photon asymmetry would basically vanish up to  $E_{\gamma}^{lab} \approx 900 \text{ MeV}$  without this resonance contribution. The branching ratio of the  $F_{15}$  resonance is also found to be well below 1%. Both resonances would have never been seen in the total cross section, because the  $S_{11}$  dominates by two orders of magnitude, and even in the angular distribution very high-precision data are required to observe the interferences with the  $s$  wave.

Our present analysis is in remarkable agreement with the calculations of Koniuk and Isgur [20] who predicted the  $\eta N$  branching ratios for the  $S_{11}(1535)$ ,  $D_{13}(1520)$  and  $F_{15}(1680)$  to be 47%, 0.09% and 0.8%, respectively, in the framework of the constituent quark model with hyperfine quark-gluon interaction. In comparison with Mukhopadhyay and Mathur [19], we confirm their finding of a much smaller ratio  $A_{3/2}/A_{1/2}$  for the  $D_{13}$  resonance than given in the Particle Data Tables and predicted by the quark model.

#### IV. SUMMARY

We have demonstrated that polarization observables are a powerful tool in analyzing individual resonances in the eta photoproduction channel. The strong dominance of the  $S_{11}$  channel allows for a more straightforward analysis than in the case of pion photoproduction. Furthermore, the nonresonant background in eta physics is small due to the weak coupling of the eta to the nucleon. A combined analysis of differential cross section, photon asymmetry and target polarization yields an almost model-independent determination of  $s$ - and  $d$ -wave multipoles. The target polarization measured at Bonn results in an unexpected phase shift between the  $S_{11}$  and  $D_{13}$  resonances that needs to be confirmed by further experiments. If this phase is taken at face value, it implies that at least one of these resonances (perhaps the  $S_{11}$ ) behaves quite differently from regular nucleon resonances and might even be a completely different phenomenon, as suggested by Ref. [18].

In conclusion, future experiments on target polarization and photon asymmetry are expected to solve another piece of the “eta” puzzle that makes this field of physics so exciting and yield qualitative new information on higher and less known structures. The photon asymmetry recently measured at GRAAL clearly indicates a contribution of the  $F_{15}(1680)$  resonance with an  $\eta N$  branching ratio of 0.15%. Similar experiments at even higher energies could help to pin down the properties of less-established resonances like the  $F_{15}(1990)$  and the  $G_{17}(2190)$ .

#### ACKNOWLEDGMENTS

We would like to thank G. Anton, J.-P. Didelez and D. Rebreyend for very fruitful discussions. This work was supported by the Deutsche Forschungsgemeinschaft (SFB201) and the US-DOE grant DE-FG02-95-ER40907.

#### APPENDIX A: HELICITY MATRIX ELEMENTS

Following the notation of Ref. [21] the helicity matrix elements for nucleon resonance production can be written as

$$\begin{aligned} A_{\frac{1}{2}}^{\ell+} &= -\frac{C_m}{\alpha} \tilde{A}_{\ell+}, \\ A_{\frac{1}{2}}^{\ell-} &= \frac{C_m}{\alpha} \tilde{A}_{\ell-}, \\ A_{\frac{3}{2}}^{\ell+} &= \frac{C_m}{2\alpha} \sqrt{\ell(\ell+2)} \tilde{B}_{\ell+}, \\ A_{\frac{3}{2}}^{\ell-} &= -\frac{C_m}{2\alpha} \sqrt{(\ell-1)(\ell+1)} \tilde{B}_{\ell-} \end{aligned} \tag{A1}$$

with

$$\alpha = \left( \frac{1}{\pi} \frac{k_R}{q_{m,R}} \frac{1}{(2J+1)} \frac{m_N}{M_R} \frac{\Gamma_m}{\Gamma_R^2} \right)^{\frac{1}{2}} \tag{A2}$$

and

$$C_m = \begin{cases} -1 & \text{for } \eta N(I = \frac{1}{2}) \\ -\sqrt{3} & \text{for } \pi N(I = \frac{1}{2}) \\ +\sqrt{\frac{2}{3}} & \text{for } \pi N(I = \frac{3}{2}) \end{cases}$$

These relations allow the extraction of the helicity elements for a resonance with mass  $M_R$ , total width  $\Gamma_R$  and total spin  $J$ . The partial decay width in the meson-nucleon decay channel  $m$  is given by  $\Gamma_m$ , and  $k_R, q_{m,R}$  are the  $cm$  momenta of the photon and the meson at the resonance position. The helicity multipoles  $\tilde{A}_{\ell\pm}$  and  $\tilde{B}_{\ell\pm}$  are defined as

$$\tilde{A}_{\ell\pm} = \text{Im}A_{\ell\pm}|_{W=M_R} \quad \text{and} \quad \tilde{B}_{\ell\pm} = \text{Im}B_{\ell\pm}|_{W=M_R} ,$$

and in general we have

$$\begin{aligned} A_{\ell+} &= \frac{1}{2}[(\ell+2)E_{\ell+} + \ell M_{\ell+}] , \\ A_{\ell-} &= \frac{1}{2}[(\ell+1)M_{\ell-} + (\ell-1)E_{\ell-}] , \\ B_{\ell+} &= E_{\ell+} - M_{\ell+} , \\ B_{\ell-} &= E_{\ell-} + M_{\ell-} . \end{aligned}$$

As introduced by Mukhopadhyay et al. [22] we can express the photoproduction multipole at resonance by the quantities

$$\xi_i \equiv \sqrt{\frac{m_N k_R \Gamma_m}{M_R q_{m,R} \Gamma_R^2}} A_i , \quad \text{for } i = 1/2 \text{ and } 3/2 . \quad (\text{A3})$$

These quantities are not sensitive to the branching ratios or total widths of the resonances. This can be easily seen by inserting Eq. (A1) into Eq. (A4),

$$\begin{aligned} \xi_{\frac{1}{2}}^{\ell+} &= -C_m \sqrt{2\pi(\ell+1)} \tilde{A}_{\ell+} , \\ \xi_{\frac{1}{2}}^{\ell-} &= C_m \sqrt{2\pi(\ell)} \tilde{A}_{\ell-} , \\ \xi_{\frac{3}{2}}^{\ell+} &= C_m \sqrt{\frac{\pi}{2} \ell(\ell+1)(\ell+2)} \tilde{B}_{\ell+} , \\ \xi_{\frac{3}{2}}^{\ell-} &= -C_m \sqrt{\frac{\pi}{2} (\ell-1)\ell(\ell+1)} \tilde{B}_{\ell-} , \end{aligned} \quad (\text{A4})$$

where only the photoproduction amplitudes at resonance enter.



- 
- [1] C. Bennhold and H. Tanabe, Nucl. Phys. A **530**, 625 (1991).
  - [2] L. Tiator, C. Bennhold and S.S. Kamalov, Nucl. Phys. A **580**, 455 (1994).
  - [3] M. Benmerrouche, N.C. Mukhopadhyay and J.-F. Zhang, Phys. Rev. D **51**, 3237 (1995).
  - [4] B. Krusche et al., Phys. Rev. Lett. **74**, 3736 (1995).
  - [5] B. Krusche et al., Phys. Lett. B **397**, 171 (1997).
  - [6] B. Schoch et al., Prog. Part. Nucl. Phys. **34**, 43 (1995).
  - [7] R. Arndt, I. Strakovsky and R. Workman, Phys. Rev. C **53**, 430 (1996).
  - [8] C. Deutsch-Sauermann, B. Friman and W. Nörenberg, Phys. Lett. B **409**, 51 (1997).
  - [9] T. Feuster and U. Mosel, Phys. Rev. C **59**, 460 (1999).
  - [10] A. Bock et al., Phys. Rev. Lett. **81**, 534 (1998).
  - [11] R. Beck et al., Phys. Rev. Lett. **78**, 606 (1997).
  - [12] J. Ajaka et al., Phys. Rev. Lett. **81**, 1797 (1998).
  - [13] G. Knöchlein, D. Drechsel and L. Tiator, Z. Phys. A **352**, 327 (1995).
  - [14] N. Kaiser, T. Waas and W. Weise, Nucl. Phys. A **25**, 297 (1997) and N. Kaiser, private communication.
  - [15] T. Feuster and U. Mosel, Phys. Rev. C **58**, 457 (1998) and T. Feuster, private communication.
  - [16] A. Bock, Ph. D. thesis, Erlangen (1997).
  - [17] Review of Particle Physics: C. Caso et al. (Particle Data Group), European Physical Journal **C3**, 1 (1998).
  - [18] G. Höhler,  $\pi$ N Newsletters **14**, 168 (1998).
  - [19] N.C. Mukhopadhyay and N. Mathur, Phys. Lett. B **444**, 7 (1998).
  - [20] R. Koniuk and N. Isgur, Phys. Rev. D **21**, 1868 (1980).
  - [21] R.A. Arndt, R.L. Workman, Z. Li and L.D. Roper, Phys. Rev. C **40**, 1864 (1990).
  - [22] N. C. Mukhopadhyay, J. F. Zhang and M. Benmerrouche, Phys. Rev. Lett. **75**, 3011 (1995).

TABLE I. Photon couplings for proton targets and multiplicities for  $N^*$  Resonances. The numbers are the averaged values from PDG98 [17] and Ref. [5] (\*).

$N^*$ Resonance	$\Gamma_R[MeV]$	helicity	$A_{1/2}, A_{3/2}[10^{-3}GeV^{-1/2}]$	$A_{\ell\pm}, B_{\ell\pm}$
$P_{11}(1440)$	$350 \pm 100$	1/2	$-65 \pm 4$	$A_{1-} = M_{1-}$
$D_{13}(1520)$	$120^{+15}_{-10}$	1/2	$-24 \pm 9$	$A_{2-} = \frac{1}{2}(3M_{2-} - E_{2-})$
		3/2	$+166 \pm 5$	$B_{2-} = E_{2-} + M_{2-}$
$S_{11}(1535)$	$150^{+100}_{-50}$	1/2	$+90 \pm 30$	$A_{0+} = E_{0+}$
	$212 \pm 20^*$		$+120 \pm 11^*$	
$S_{11}(1650)$	$150^{+40}_{-5}$	1/2	$+53 \pm 16$	$A_{0+} = E_{0+}$
$D_{15}(1675)$	$140^{+30}_{-10}$	1/2	$+19 \pm 8$	$A_{2+} = 2E_{2+} + M_{2+}$
		3/2	$+15 \pm 9$	$B_{2+} = E_{2+} - M_{2+}$
$F_{15}(1680)$	$130 \pm 10$	1/2	$-15 \pm 6$	$A_{3-} = 2M_{3-} - E_{3-}$
		3/2	$+133 \pm 12$	$B_{3-} = E_{3-} + M_{3-}$

TABLE II. Parameterization and fitted values from our energy-dependent analysis for the coefficients a, b, c, d, e, f and g. Each of the coefficients is parameterized in the form  $\sum_i \alpha_i (q_\eta^{cm}/m_\eta)^{n_i}$  with up to 3 terms. The coefficients a, b, c have the dimension of a cross section [ $\mu b$ ], all others are dimensionless.

	$n_1$	$\alpha_1$	$n_2$	$\alpha_2$	$n_3$	$\alpha_3$
a	0	$4.59 \pm 0.04$	2	$-9.33 \pm 0.52$	-	-
b	1	$-0.29 \pm 0.07$	-	-	-	-
c	2	$-4.82 \pm 0.46$	-	-	-	-
d	1	$0.16 \pm 0.03$	-	-	-	-
e	2	$9.6 \pm 2.3$	3	$-38.3 \pm 10.$	4	$36.4 \pm 10.$
f	2	$1.70 \pm 0.10$	4	$-1.38 \pm 0.32$	-	-
g	6	$-10.4 \pm 2.8$	8	$30.7 \pm 6.4$	-	-

TABLE III. Resonance properties determined by our analysis. The first line for each resonance is taken from the Particle Data Tables 1998 [17]. Our analyses (case 1 and 2) are based on the average values from PDG for the mass  $M_R$ , full width  $\Gamma_R$  and  $A_{3/2}$ , see Tab. II .

$N^*$ Resonance	$b_\eta = \Gamma_\eta/\Gamma_R$ [%]	$A_{1/2}$ [ $10^{-3}/\sqrt{GeV}$ ]	$A_{3/2}/A_{1/2}$	$\xi_{3/2}$ [ $10^{-4}/MeV$ ]	$\xi_{1/2}$ [ $10^{-4}/MeV$ ]
$D_{13}(1520)$	-	$-24 \pm 9$	$-6.9 \pm 2.6$	-	-
case 1	$0.08 \pm 0.01$	$-79 \pm 9$	$-2.1 \pm 0.2$	$0.185 \pm 0.018$	$-0.087 \pm 0.013$
case 2	$0.05 \pm 0.02$	$-79 \pm 9$	$-2.1 \pm 0.2$	$0.134 \pm 0.018$	$-0.087 \pm 0.013$
Ref. [19]	-	$-79 \pm 9$	$-2.5 \pm 0.2 \pm 0.4$	$0.167 \pm 0.017$	$-0.066 \pm 0.008$
Ref. [20]	0.09	-23	-5.56	-	-
$F_{15}(1680)$	-	$-15 \pm 6$	$-8.9 \pm 3.6$	-	-
case 2	$0.15^{+0.35}_{-0.10}$	-	-	$0.16 \pm 0.04$	-
Ref. [20]	0.8	0.0	-	-	-

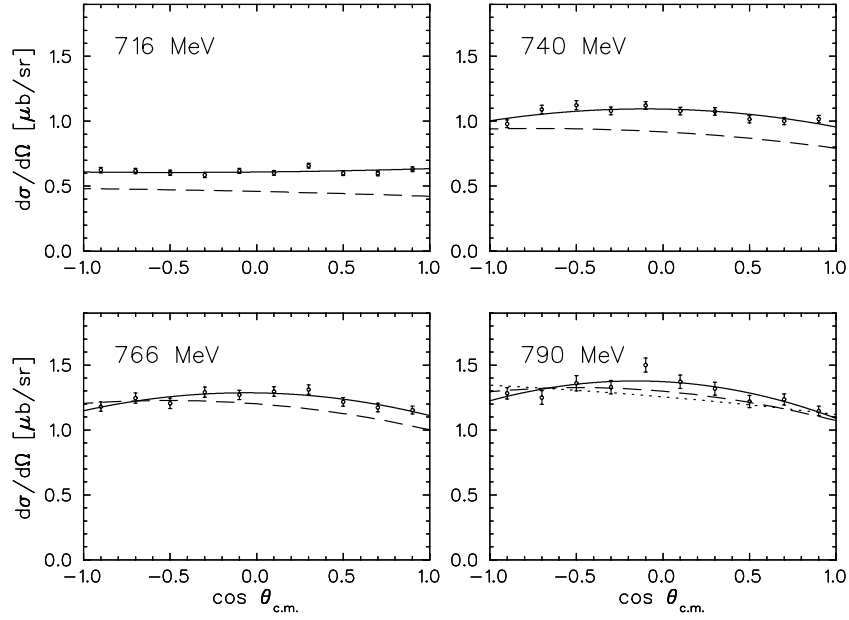


FIG. 1. Differential cross sections for  $p(\gamma, \eta)p$  at various photon *lab* energies  $E_{\gamma}^{lab}$ . The solid lines show our fit to the experimental data of Krusche et al. [4]. The dashed lines are the values of the isobar model of Knöchlein et al. [13] and the dotted line at  $E_{\gamma}^{lab} = 790 \text{ MeV}$  is obtained from this model if the  $D_{13}$  resonance is turned off.

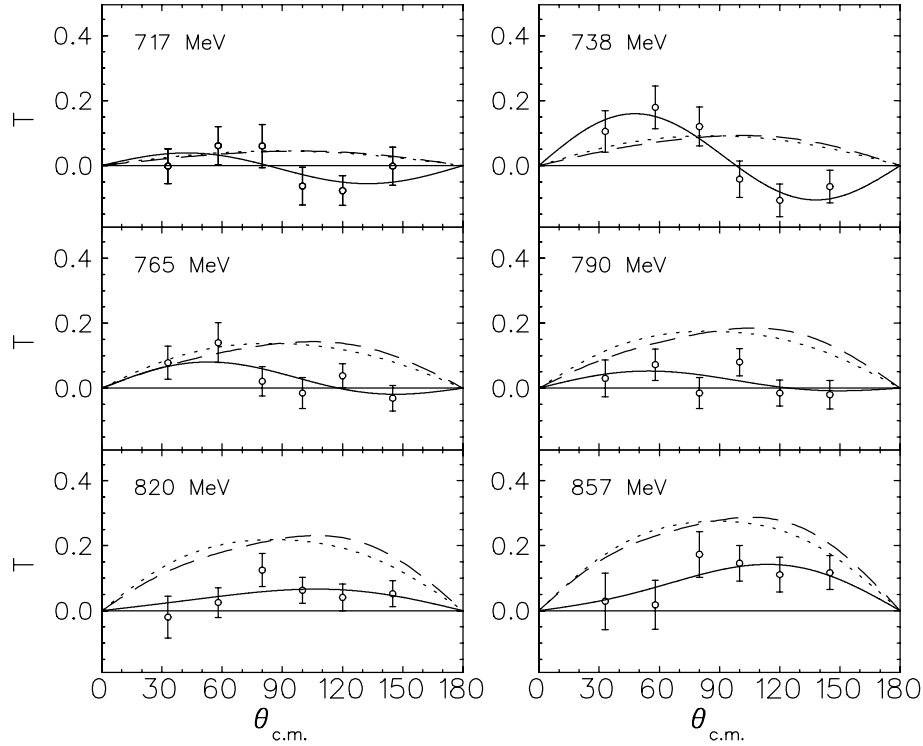


FIG. 2. Target asymmetries for  $p(\gamma, \eta)p$  at various photon *lab* energies  $E_{\gamma}^{lab}$ . The dashed and dotted lines show calculations in the isobar model of Knöchlein et al. [13] with and without the  $D_{13}(1520)$  resonance. The solid line is the result of our fit to the experimental data of Bock et al. [10].

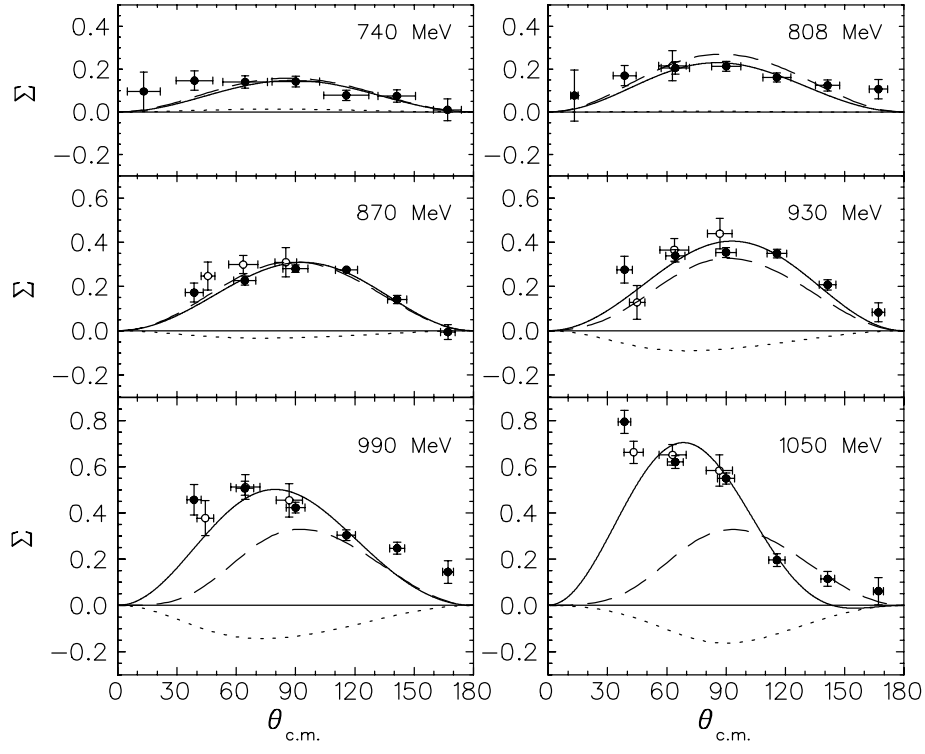


FIG. 3. Photon asymmetries for  $p(\gamma, \eta)p$  at various photon *lab* energies  $E_{\gamma}^{lab}$ . The dashed and dotted lines show calculations in the isobar model Knöchlein et al. [13] with and without the  $D_{13}(1520)$  resonance. The solid line is the result of our fit to the experimental data of Ajaka et al. [12].

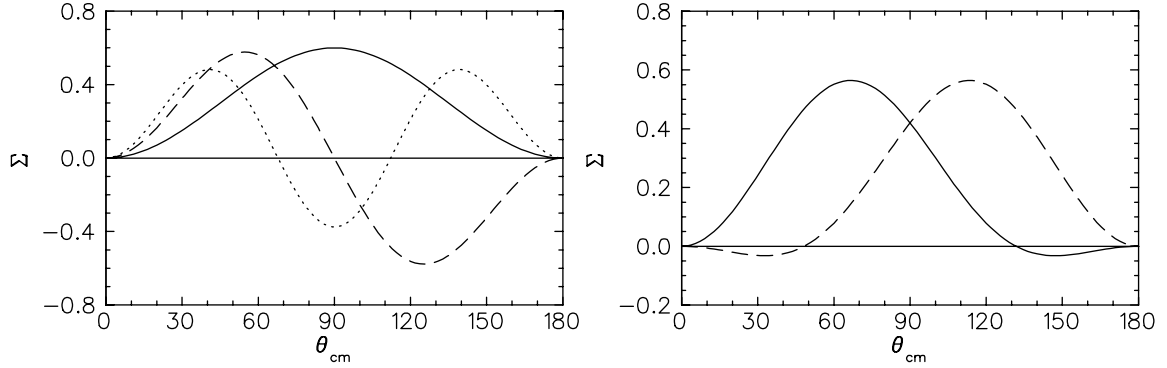


FIG. 4. Possible signatures of  $N^*$  resonances in the photon asymmetry of eta photoproduction. The solid, dashed and dotted lines in the left figure show the angular distributions for the interference of the dominant  $S_{11}$  channel with an isolated  $d$ ,  $f$ , or  $g$  wave, respectively. Opposite signs are obtained if the photon or eta couplings of the higher resonances carry an opposite sign, see Table I. On the right, the situation of two overlapping resonances is demonstrated for a  $(D_{13}, F_{15})$  pair (solid curve) and a  $(D_{13}, F_{17})$  pair (dashed curve).

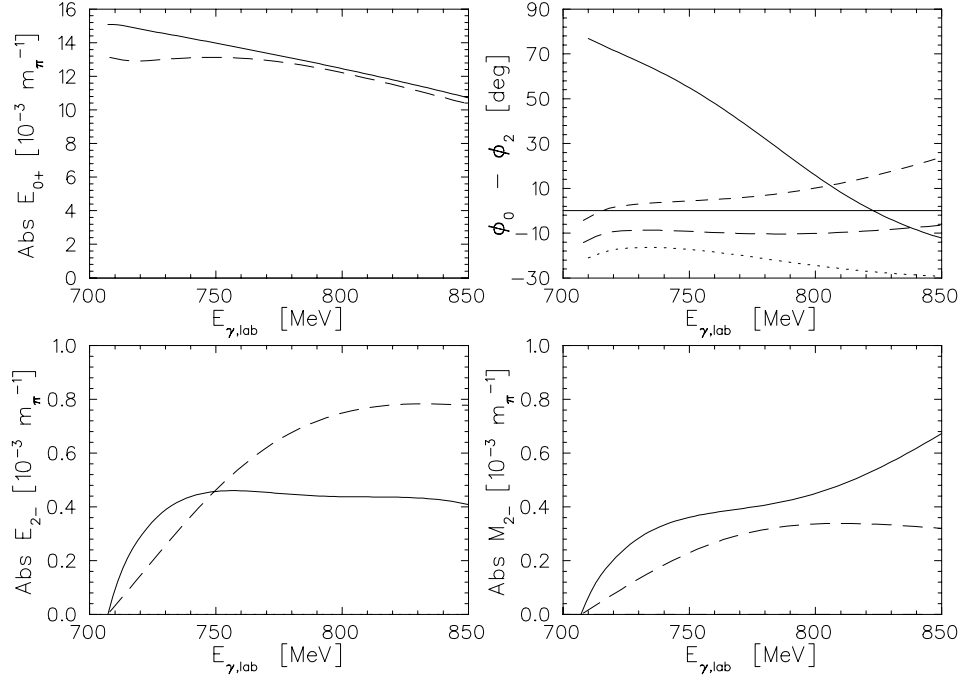


FIG. 5. Result of the multipole analysis for  $s$  and  $d$  waves. The solid lines show the result of our fit. The short and long dashed lines are obtained using the isobar model of Ref. [13]. In the upper right figure we compare the phase difference of our fit with the isobar model. The short and long dashed curves show  $\phi_{E_{0+}} - \phi_{E_{2-}}$  and  $\phi_{E_{0+}} - \phi_{M_{2-}}$ , respectively, and the dotted line is the phase difference for two Breit-Wigner forms.

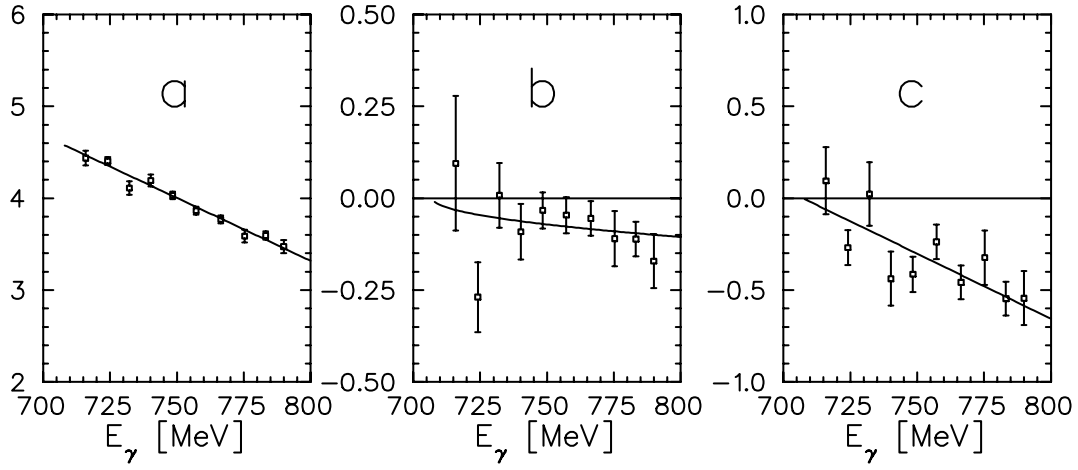


FIG. 6. Fit coefficients  $a$ ,  $b$  and  $c$  for the differential cross section measured at Mainz [4]. The solid lines show polynomial fits allowing for an energy dependent solution. The coefficients are given in units of  $\mu\text{b}/\text{sr}$ .

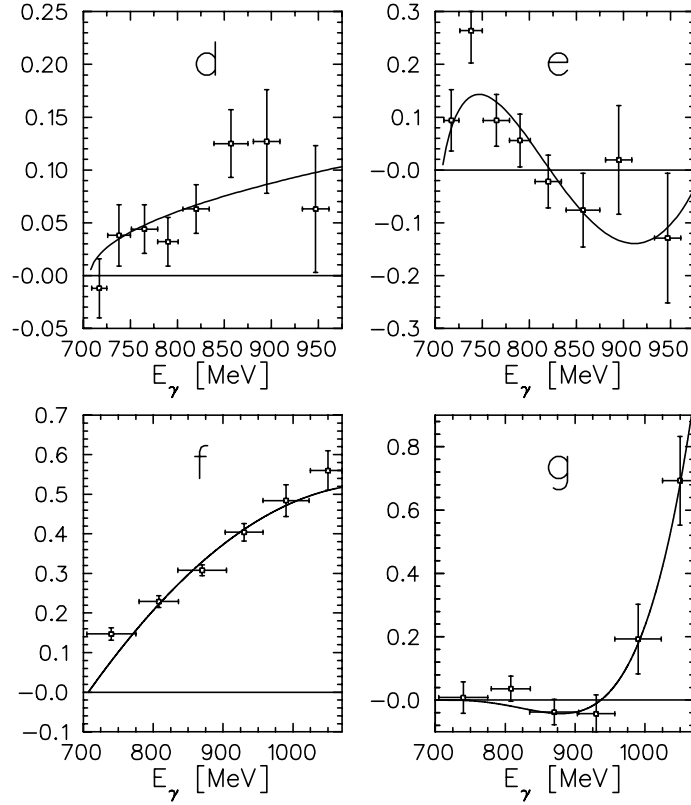


FIG. 7. Fit coefficients  $d$ ,  $e$ ,  $f$  and  $g$  of the target and beam asymmetry measured at Bonn [10] and GRAAL [12]. The solid lines show polynomial fits allowing for an energy dependent solution. The coefficients are dimensionless.